Adsorption (2015) 21:565–575
DOI 10.1007/s10450-015-9700-x

CO_2/CH_4 adsorption separation process using pore expanded mesoporous silicas functionalizated by APTES grafting

E. Vilarrasa-García[1,2] · J. A. Cecilia[2] · M. Bastos-Neto[1] · C. L. Cavalcante Jr.[1] · D. C. S. Azevedo[1] · E. Rodriguez-Castellón[2]

Received: 31 August 2015 / Revised: 5 October 2015 / Accepted: 5 October 2015 / Published online: 11 October 2015

Abstract In this work we have studied the CO_2 adsorption capacity and CO_2/CH_4 separation on several APTES-grafted mesoporous silicas of SBA-15 type. The synthesis was modified in order to obtain pore expanded materials, and post synthesis functionalization was carried out by grafting with APTES (by immersion in 20 % v/v solution). The samples were characterized by elemental (CNH) analysis, X-ray diffraction, N_2 adsorption–desorption isotherms at −196 °C, and TGA. To test the CO_2 adsorption capacity and CO_2/CH_4 separation of all samples, a gravimetric method with a magnetic suspension balance (Rubotherm, Germany) was used. Monocomponent and mixture adsorption isotherms were measured at 25 °C. All isotherms were recorded to 10 bar. Monocomponent experimental data were fitted to Langmuir and Dual-site Langmuir models and the mixture experimental data were well fitted to Multiregion Extended Langmuir combined with Dualsite Langmuir model, achieving a good correlation between experimental and simulated data.

Keywords CO_2 · Adsorption · Mesoporous silicas · Equilibrium models · Selectivity · CH_4

✉ D. C. S. Azevedo
diana@gpsa.ufc.br

✉ E. Rodriguez-Castellón
castellon@uma.es

[1] Departamento de Engenharia Química, GPSA-Grupo de Pesquisa em Separações por Adsorção, Universidade Federal do Ceará, Campus do Pici, Fortaleza, Ceará 60455-760, Brazil

[2] Departamento de Química Inorgánica, Facultad de Ciencias, Universidad de Málaga, 29071 Málaga, Spain

1 Introduction

Carbon dioxide is released from the activity of animals, plants, and microorganisms and is consumed by photosynthesis and oceanic dissolution (EPA. Inventory of U.S. Greenhouse Gas Emissions and sinks: 1990–2006 2008, Lackner et al. 2009). These large natural sources and sumps are in quasi balance. However, anthropogenic emissions from fossil fuel combustion, especially in the last century, are cause of concern because they have disturbed this natural carbon balance, increasing levels of atmospheric CO_2 to above 400 ppm (IPCC). This rise has been linked to global warming and ocean acidification, and will grow together with increasing fossil fuel consumption required to meet the world's energy demand. Rising concerns of the effects that anthropogenic CO_2 has on global climate change has led to the introduction of schemes for mitigation carbon emissions and/or research and development of alternative energy sources. Globally, 85 % of energy is derived from fossil fuels (Lackner et al. 2009) and the global energy demand is expected to have increased by 30 % in 2040 (ExxonMobil, The Outlook for Energy: A View to 2040, 2012). A decline in global fuel dependence will necessarily come together with the development of more effective methods of CO_2 capture. Current methods of CO_2 removal from flue gases have had some industrial success, using alkanolamines (monoethanolamine (MEA), diethanolamine (DEA) and methyl diethanolamine (MDEA)) in chemical absorption systems. (Wolsky et al. 1994; Veawab et al. 2002). These absorption processes are among the most mature and effective; however, a large amount of energy is required for regeneration, resulting in considerable reductions in the net power plant output. While suggestions have been proposed to improve the efficiency of the processes, it is clear that a

more drastic step forward is needed if any real advance towards a universal and low-cost CO_2 sequestration system is to be achieved.

Methane, either from natural gas or biogas, is indicated to achieve the highest growth rate of all current energy sources. This is due to the discovery of new offshore fields, the limited environmental impact and more efficient combustion methods. In fact, when the amount of carbon dioxide emitted by burning different fuels is considered, biogas and natural gas appear at the bottom of the list, with 0.25 kg of CO_2 emitted per million calories, whereas gasoline emits almost 0.36 and coal from different sources emits above 200 (EIA, U.S. Energy Information Administration. www.eia.gov). By 2020, natural gas use is expected to exceed coal consumption, which is continually being penalized by stricter emission limits (Tagliabue et al. 2009). Nevertheless, treatment of raw gas will always be required either for transportation, or to increase the calorific power for efficient combustion. This treatment requires removal of contaminants of which carbon dioxide is the most abundant.

With this respect, solid adsorbents such as zeolites, activated carbons, metal organic frameworks, alkaline oxides and organic/inorganic hybrids have been widely reported (Wang et al. 2011). The functionalization of some of these materials with amine sources leads to higher CO_2 affinity and selectivity. Thereby organosilanes like (3-aminopropyl) triethoxysilane by grafting (Vilarrasa-García et al. 2014) or tetraethylenepentamine (Sanz-Perez et al. 2013) by impregnation are commonly used. Recently, silica with amidoxime groups also has been reported as promising CO_2 adsorbent at relatively high temperature (Gunathilake and Jaroniec 2014).

The introduction of ordered mesoporous material MCM-41 in 1992 (Beck et al. 1992) led to the synthesis of different mesoporous materials with high specific surface area and thermal stability. Some years later, in 1998, SBA (Santa Barbara) series of ordered mesoporous silica was synthesized using a neutral triblock template agent (Zhao et al. 1998a, b). The synthesis is performed by different interactions in an aqueous medium between an inorganic phase (silicon precursor) and another organic surfactant, which acts as the structure director agent. This group of materials, especially SBA-15, attracted researchers' attention due to its outstanding properties. For example, it has a relatively high specific surface area and uniform pore size. In addition, the silica wall is as thick as 3 nm or larger and therefore it has high hydrothermal stability (Zhao et al. 1998a, b). There are also micropores crossing silica walls, through which the mesopore channels are interconnected (Ryoo et al. 2000). The pore size is adjustable for a wide range, between 5-30 nm, using organic swelling agents such as trimethylbenzene (Zhao et al. 1998a, b; Schmidt-Winkel et al. 1999), trisiopropylbenzene (Cao et al. 2009), among others. Research on potential applications of these materials has been actively carried out (Chang et al. 2003; Fornés et al. 2003; Newalkar et al. 2003), including gas separation and storage. Utilization of alternative fuels is an urgent task due to a rapidly increasing oil price. Natural gas or other methane-containing fuels can be used in vehicles with fairly clean emissions.

In this work, the CO_2 adsorption capacity and CO_2/CH_4 separation on several APTES-grafted mesoporous silicas of SBA-15 type were studied.

2 Experimental

2.1 Synthesis of adsorbents

The synthesis of SBA-15 type silica was performed using hydrothermal treatment as described by Fulvio et al. (2005) with some modifications. Four synthesis routes were studied and the materials thus prepared were labeled as SBA15, STMB, SHEPF and STMBF.

In the first synthesis, 4 g of Pluronic 123 (P123) were dissolved in 144 mL HCl solution (1.7 M) under stirring until complete dissolution of the surfactant was achieved. Then, 8.75 mL of tetraethyl orthosilicate (TEOS) were added under stirring for 24 h at 40 °C. The prepared solid was denoted as SBA15. The final molar composition for the synthesis gel was set to $P123/SiO_2/HCl/H_2O = 1/55/350/11100$.

In the case of the second SBA-15 type silica, denoted as STMB, the synthesis was performed by adapting the hydrothermal synthesis described by Fulvio et al. (2005). P123 was firstly dissolved in 1.7 M HCl (aq.) at 40 °C, and then trimethylbenzene (TMB) was also added as a swelling agent into the transparent solution. After 30 min, TEOS was added dropwise. The final molar ratio in the synthesis gel was $P123/SiO_2/TMB/HCl/H_2O = 1/55/48/350/11100$.

The third and fourth SBA-15 silica (labeled as SHEPF and STMBF) were synthesized like SBA15 and STMB, but by adding ammonium fluoride (0.045 g) as a solubility enhancer together with the addition of P123. Additionally, 22 mL n-heptane (SHEPF), instead of TMB, were added simultaneously with TEOS. P123 and NH_4F were dissolved in 1.7 M HCl (aq.) at 40 °C. In turn, TEOS was premixed with *n*-heptane and added into the transparent solution with further stirring for 24 h at the same temperature (SHEPF). In the case of STMBF, TMB was added 30 min before the TEOS addition. The final molar ratio in the synthesis gel were $P123/SiO_2/HCl/NH_4/heptanes/H_2O = 1/55/350/1.8/235/11100$ and $P123/SiO_2/TMB/HCl/NH_4/H_2O = 1/55/48/350/11100$ for SHEPF and STMBF, respectively. The presence of ammonium fluoride in the synthesis gel has

been described in previous publications as a polycondensation catalyst of the silicon precursor (Boissière et al. 2000a, b; Vilarrasa-Garcia et al. 2015).

In all cases, the synthesis gels were transferred to a Teflon lined reactor and placed in an autoclave. The reactor was sealed and heated at 120 °C for 72 h. The solids were filtered, washed with water/ethanol and dried at 60 °C for 24 h. The dried solids were then calcined at 550 °C at a heating rate of 1 °C min^{-1}, and kept at this temperature for 6 h.

The *grafting* of APTES in each support was carried out following the methodology reported by Hiyoshi et al. (2004). 1 g of the support, previously dried at 120 °C in N_2 atmosphere, was introduced in a three-neck flask with 20 % vol. of a solution of APTES in toluene (50 mL). The solution was then refluxed at 110 °C in N_2 atmosphere. After 12 h, the solid was filtered and washed with toluene and air dried at 120 °C.

2.2 Material characterization

X-ray powder diffraction (XRD) was used to identify structural changes in the SBA framework caused by the use of different swelling agents. These measurements were performed on an X'Pert Pro MPD automated diffractometer equipped with a Ge (111) primary monochromator (strictly monochromatic Cu-Kα radiation, $\lambda = 1.5406$ Å) and an X'Celerator detector. Measurements were obtained for 2 h in the range of 1–10°.

The textural parameters (S_{BET}, V_P and D_P) were estimated from nitrogen adsorption–desorption isotherms at −196 °C using an automatic ASAP 2020 system from Micromeritics. Prior to the measurements, samples were outgassed at 120 °C and 10^{-4} mbar overnight. Surface areas were determined by using the Brunauer–Emmett–Teller (BET) equation (Brunauer et al. 1938) assuming a cross section of 16.2 $Å^2$ for the nitrogen molecule. The pore size distribution was calculated by applying the Barrett–Joyner–Halenda (BJH) method (Barrett et al. 1951) applied to the desorption branch of the N_2 isotherm. The total pore volume was calculated from adsorbed N_2 at $P/P_0 = 0.996$.

Thermal analysis was performed on a TG-DTG thermobalance (Mettler Toledo) with a continuous heating rate of 10 °C min^{-1} in a synthetic air atmosphere (flowing at 50 mL min^{-1}).

Elemental chemical analysis was performed with a LECO CHN 932 analyzer to determine the nitrogen, carbon and hydrogen content.

2.3 Adsorption measurements

Single gas CO_2, CH_4 and binary gas CO_2/CH_4 adsorption measurements were performed using a Rubotherm (Bochum, Germany) magnetic suspension balance equipped with a gas mixture dosing unit. Around 0.5 g of each sample were used in the balance. Prior to each measurement, samples were outgassed at 120 °C for 2 h (heat rate 1 °C/min) under vacuum. The regenerated samples were exposed to pure (or mixed) gas at constant temperature. The change in weight of the samples with respect to pressure and temperature was measured continuously until equilibrium was reached. The condition to satisfy equilibrium was a mass variation of less than 10^{-4} g for 30 min. A correction for the buoyancy effect was performed by helium measurements at 25 °C in the pressure range of 0–10 bar so as to allow for the determination of the excess adsorbed concentration. The temperature during the adsorption isotherms was held constant by using a thermostat bath.

The quantity of mass adsorbed was calculated by application of Eq. (1):

$$m_{exc} = \Delta m + \rho \cdot (V_b + V_s) \quad (1)$$

where m_{exc} is the excess adsorbed concentration, Δm is the mass difference between the mass at each pressure and the mass under vacuum (after regeneration), ρ is the density (at a fixed pressure and temperature) of the fluid gas surrounding the adsorbent. Density was obtained in either two ways: from equations of state (CO_2 (Span and Wagner 1996), CH_4 (Setzmann and Wagner 1991), He (McCarty and Arp 1990)) or experimentally by direct measurements using the balance.

Isotherms were obtained in the pressure range of 0-10 bar. Within this range the deviations between excess adsorbed concentration and absolute adsorbed concentration for CO_2 and CH_4 are negligible (Dreisbach et al. 1999) and hence no correction to the experimental values were required for the sake of comparison with predictive equilibrium models. No adsorption–desorption cycles are described in this work due to it was shown in previous works that these amino functionalized silicas can be subjected to several adsorption–desorption cycles holding their CO_2 capacity. (Heydari-Gorji et al. 2011; Vilarrasa-García et al. 2014; Jing et al. 2014).

3 Equilibrium models for multicomponent adsorption

In this work, the extended Langmuir (EL) model was used to describe mixed gas adsorption behavior due to its simplicity. In this model, the basic assumptions of the Langmuir theory are applied to each component. These assumptions imply that the adsorbent surface has a specific number of sites where the solute molecules can be

adsorbed; these sites have the same adsorption energy for all molecules of a given gas; and there is no interaction between adsorbed molecules.

Considering that the adsorption rate for a particular component is proportional to its partial pressure in the gas phase and also to the fraction of vacant sites, equating both rates of adsorption and desorption, then summing for all components, yields the following Eq. (2) in terms of the adsorbed concentration in equilibrium. The rate of desorption of the same component is assumed to be proportional only to its fractional loading, so that it is independent from the fractional loadings of other components:

$$q = \frac{q_{m,i} \cdot b_i \cdot p_i}{1 + \sum_{j=1}^{N} b_j \cdot p_j} \tag{2}$$

where b_i is the ratio of the adsorption and desorption rate constants, as estimated from pure gas adsorption data, and it qualifies the affinity of the adsorbent surface for a given the component i.

However, the EL model is not thermodynamically consistent, unless the saturated quantity adsorbed in the pure component isotherm is the same for all components present in the mixture (Yang 1987; Bai and Yang 2001). The Multi Region Extended Langmuir (MREL) was also applied to fit binary equilibrium adsorption isotherms. The MREL model assumes the existence of two different types of adsorption sites. One of them, namely site 1, can be occupied by both components and the other one, site 2, only can be occupied only by one component. The component exclusion for this type of site is attributed to the absence of competition. For the sake of thermodynamic consistency, the saturation capacity (q_m) of both gases is assumed to be the same for site 1. Hence, the EL model may be used to predict the adsorption equilibrium of the mixture on site 1. On site 2 however, only species A (CO_2 in our case) can be adsorbed and molecule B (CH_4 in this paper) is excluded for the reasons previously discussed. As a consequence, the total amount of component A adsorbed is the sum of the amount adsorbed on site 1 and 2, whereas the total amount adsorbed of B is the quantity adsorbed only on site B. Model equations are described as follows:

On site 1:

$$q_{A,1} = \frac{q_{m,B} \cdot b_A \cdot p_A}{1 + b_A \cdot p_A + b_B \cdot p_B} \tag{3}$$

$$q_{B,1} = \frac{q_{m,B} \cdot b_B \cdot p_B}{1 + b_A \cdot p_A + b_B \cdot p_B} \tag{4}$$

On site 2:

$$q_{A,2} = \frac{(q_{m,A} - q_{m,B}) \cdot b_A \cdot p_A}{1 + b_A \cdot p_A} \tag{5}$$

$$q_{B,2} = 0 \tag{6}$$

And the total amount adsorbent for each component is:

$$q_A = q_{A,1} + q_{A,2} \tag{7}$$

$$q_B = q_{B,1} \tag{8}$$

Finally, the Dual-Site Langmuir model (DSL) was also applied to fit experimental data. This takes into account that CO_2 is adsorbed on site 1 and site 2. From the fit of the DSL we can distinguish between b values for both CO_2 adsorption sites.

$$q_{CO_2} = \frac{q_{m,1} \cdot b_1 \cdot p_1}{1 + b_1 \cdot p_1} + \frac{q_{m,2} \cdot b_2 \cdot p_2}{1 + b_2 \cdot p_2}. \tag{9}$$

To estimate the accuracy of each fit of the proposed models, a deviation function based on the difference of the experimental and estimated amount adsorbed was used:

$$D(\%) = \frac{1}{N} \sum_{i=1}^{Nt} \frac{q_{i,est} - q_{i,exp}}{q_{i,exp}} \cdot 100 \tag{10}$$

where N_t is the number of the data points, and $q_{i,est}$ and $q_{i,exp}$ are the estimated and experimental amounts adsorbed in a mixture, respectively.

4 Results and discussion

The XRD patterns (low angle) for the four synthesized silica samples before and after APTES functionalization (20 % vol. APTES) are shown in Fig. 1. Conventional

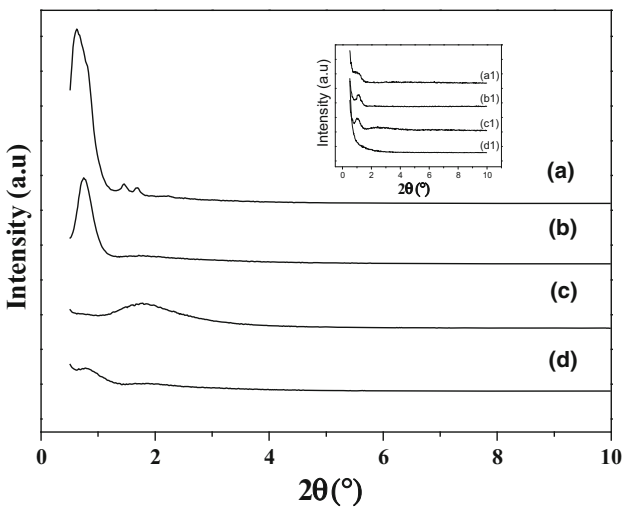

Fig. 1 XRD patterns for *a* SBA-15, *b* TMB, *c* HEPF and *d* TMBF. Top right corner XRD patterns for grafted silicas *a1* S15, *b1* STMB, *c1* SHEPF, *d1* STMBF

SBA-15 showed three well resolved peaks that can be identified as (100), (110) and (200) reflections associated with the p6 mm hexagonal symmetry, in agreement with previous works (Zhao et al. 1998a, b; Kruk et al. 2000; Celer and Jaroniec 2006). For the pore expanded supports, these peaks could not be identified, suggesting a more disordered pore structure. From XRD patterns, it can be concluded that the structural ordering of synthesized materials decreases in the presence of swelling agents. With regard to the samples synthesized with fluoride (HEPF and TMBF), several authors (Schmidt-Winkel et al. 1999; Lettow et al. 2000; Schmidt-Winkel, et al. 2000; Zhang et al. 2004) have established that the presence of fluoride limits the growth of the channels, leading to materials with a shorter length of mesochannels. Fluoride presence also gives an inferior long-range order as indicated by a great decrease in the intensity of the reflection lines with respect to that observed in the diffractogram of conventional SBA-15.

Figure 2 shows the N_2 adsorption–desorption isotherms at −196 °C of all starting siliceous adsorbents. A clear difference is observed for pore expanded supports, as the capillary condensation in mesopores appears at a higher relative pressure than that observed in the case of conventional SBA-15 materials (SBA-15).

Table 1 summarizes the textural properties of the studied materials. As expected, the BJH average pore size exhibits a significant increase with the addition of swelling agents (pore diameter values above 12 nm). Specific surface area determined by the BET equation showed that the surface area of conventional SBA is higher than that of expanded materials. All isotherms are type IV, according to IUPAC nomenclature with H1 type hysteresis loops indicative of cylindrical pore shape, although the hysteresis for expanded silicas are poorly defined.

Table 1 Textural properties of pure silicas. Textural properties for amino grafted silicas are shown in parenthesis

	S_{BET} (m^2/g)	Vp (cm^3/g)	Dp (nm)	%N
SBA-15	730 (225)	1.35 (0.46)	8 (6)	3.91
STMB	432 (191)	1.51 (0.74)	17 (12)	4.11
SHEPF	433 (109)	1.33 (0.78)	16 (13)	5.32
STMBF	460 (120)	2.68 (0.70)	18 (15)	5.53

N content (%) of functionalized silicas are included as determined by elemental analysis for amino grafted silicas

V_p: total pore volume was calculated from adsorbed N_2 at $P/P_0 = 0.996$

Figure 3 shows the TG curves of all materials. TG curves exhibit a first stage weight loss below 200 °C caused by the release of moisture, adsorbed gases and free APTES molecules (Wang and Yang 2011; Zelenak et al. 2008; Kishor and Ghoshal 2015). Samples synthesized with STMB as an expander agent present a similar weight loss (around 4 % below 150 °C) whereas conventional SBA-15 (more ordered) shows a higher water affinity, which may be due to the interactions between silanol groups and water molecules by hydrogen bonds (Vilarrasa-Garcia et al. 2015). For amine grafted silicas, the synthesis route has a significant impact on the amine grafted over the surface. Although all samples were grafted with the same quantity of aminosilane, STMBF and HEPF were the samples that retained a higher quantity of amine groups, and this may be due the major accessibility of the APTES molecules to the silanol groups. These results are in agreement with elemental analysis (Table 1), where STMBF and SHEPF reached a N content of 5.32 and 5.54 %, respectively. Fluoride limits the growth of mesochannels so APTES access to silanols is easier and thereby the grafting performance is higher.

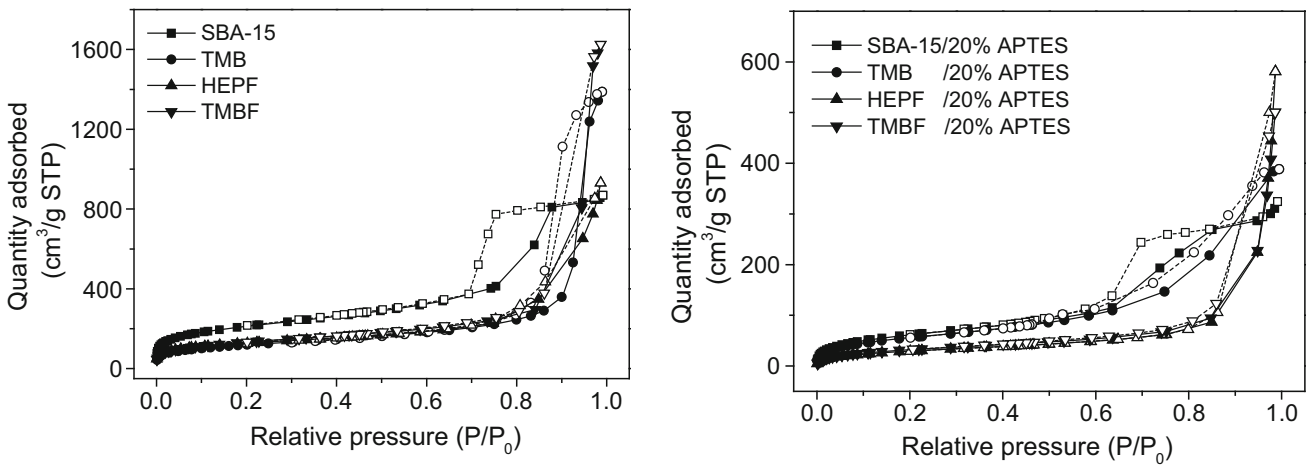

Fig. 2 N_2 adsorption–desorption isotherms at −196 °C. On left pure silicas and on right grafted silicas

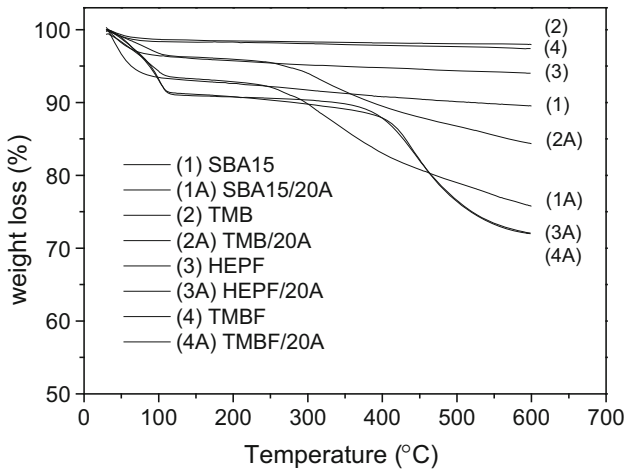

Fig. 3 TG curves for *1* SBA15, *2* STMB, *3* SHEPF, *4* STMBF. Also in Figure are plotted TGA curves for amino grafted silicas, labeled as NA, being N a number between 1 and 4 which corresponds with starting samples

Specific volume of adsorbents was determined by measurements with helium at room temperature in the pressure range of 0–10 bar. No significant difference was observed in the specific volumes obtained for different materials, ranging around 0.5–0.6 cm^3/g.

Monocomponent adsorption isotherms were obtained for CO_2 and CH_4 at 25 °C up to 10 bar. In Fig. 4, CO_2 and CH_4 adsorption isotherms are plotted, as well as molar ratio $CO_2/CH_4 = 1$ adsorption isotherm and the fits of experimental data to Extended Langmuir (EL), Multiregion Extended Langmuir (MREL) and MREL using Dualsite (MREL DsL) to discriminate between CO_2 adsorption constants for the two sites of adsorption.

The highest CO_2 capacities were obtained for samples that showed a superior grafting yield, i.e. SHEPF and STMBF. These samples reached 2.85 and 2.65 mmol CO_2/g at 25 °C and 10 bar, while conventional SBA-15 and STMB adsorbed 2.44 and 2.30 mmol CO_2/g, respectively. However, the greatest difference in terms of adsorbed concentration was observed at low pressures, where less ordered samples showed a higher capacity of CO_2 (2.39 mmol CO_2/g for SHEPF at 25 °C and 1 bar). The presence of a higher density of amine groups has a direct impact on the shape of isotherm, leading to a more favorable equilibrium. Amine groups react with CO_2 molecules through the Zwitterion mechanism, with the formation of ammonium carbamate in anhydrous conditions, which is reflected in the highest values for *b* (see Tables 2 and 3). With regards to methane adsorption, all samples adsorbed similar quantities. CH_4 isotherms show nearly linear behavior, indicating a lower affinity of these amine-silicas towards CH_4.

Experimental mixture isotherms with a molar ratio $CO_2/CH_4 = 1$ were also obtained at 25 °C. As expected, SHEPTF showed a higher quantity of adsorbed CO_2 as it was observed in monocomponent measurements. All binary gas isotherms were fit using EL and MREL with parameters estimated from fitting monocomponent equilibrium data to Langmuir model (Table 3). The aim of these fits is to find a tool that allows us to predict isotherms with different CO_2/CH_4 ratios from experimental data of pure components and to foresee the behavior of the materials in several scenarios.

Therefore, in order to find a model that most accurately predict CO_2/CH_4 binary gas adsorption data, the Langmuir model was used to fit the monocomponent isotherms for the experimental data of CO_2 and CH_4. From this, a comparison was conducted using the several models to fit experimental data of mixtures obtained gravimetrically.

Generally, the EL model shows higher deviations, whereas the MREL better predicts binary gas experimental data. However, the MREL model considers that CO_2 can be adsorbed on two different sites and uses the same adsorption constant (b) for both sites. We propose in this paper the use of Dualsite Langmuir model to find the adsorption constant values of these likely sites for CO_2 adsorption, so monocomponent CO_2 isotherms are fitted to Dualsite Langmuir model. Based on previous works (Vilarrasa-García et al. 2014), we have assumed that site 2 is the one with the higher value of b. Site 2 binds more strongly than site 1, which is related to the presence of amine groups. Therefore, site 2 only adsorbs CO_2 and site 1 can adsorb both CO_2 or CH_4, keeping the same q_m obtained to fit CH_4 data by application the Langmuir model. From these considerations, MREL with DsL for CO_2 is able to predict experimental more accurately data than EL or MREL (see Table 3).

From the fit of MREL applying the DsL model, several mixture isotherms were simulated by varying the partial pressure of CO_2 and CH_4 (Fig. 5). From this, binary gas equilibrium adsorption isotherms were obtained with a range of compositions from 50 to 90 % CH_4. The aim of this study is to check if these materials have the same trend when the mixture evolves towards natural gas scenarios. All samples showed a decrease in the gravimetric uptake as the CH_4/CO_2 ratio increases however, just as expected, samples with a higher %N content maintain a good CO_2 uptake (above 0.7 g/g with a mixture 30 % CO_2 70 % CH_4 at 10 bar and 25 °C). In terms of selectivity, MREL combined with DsL predicts a decreasing selectivity as pressure increases. STMBF and SHEPF were the samples that exhibited the highest selectivity, decreasing from around 195 and 150 mol CO_2/mol CH_4 at 0.2 bar until 180 and 155 mol at 10 bar, respectively. SBA15 and STMB showed lower values, decreasing from 29 and 32 mol

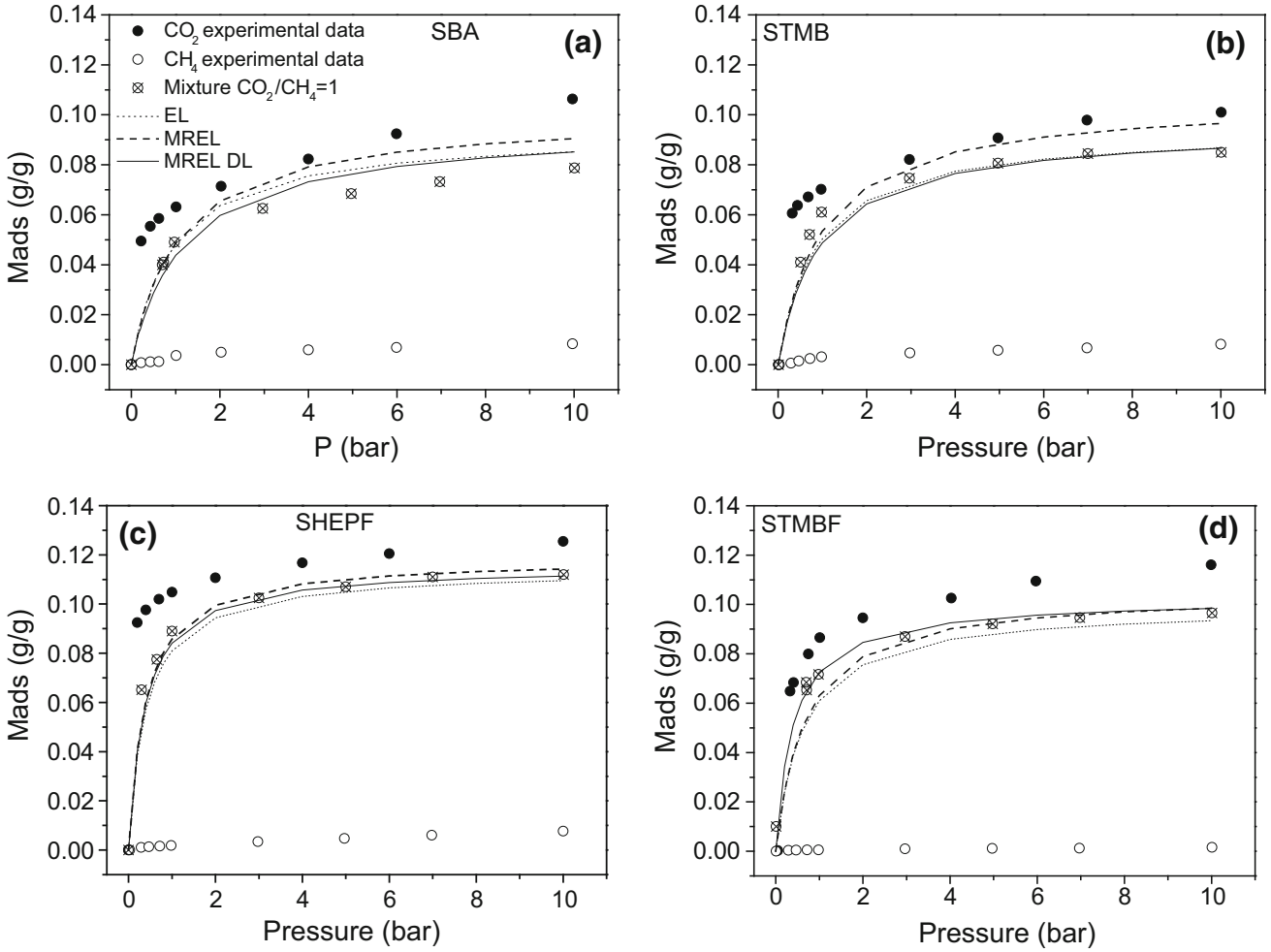

Fig. 4 CO_2 (*circle*), CH_4 (*empty circle*) and $CO_2/CH_4 = 1$ (*stripped circle*) experimental isotherms at 25 °C for **a** SBA-15, **b** TMB, **c** HEPF, **d** TMBF. Fits to Extended Langmuir (*dotted line*), MultiRegion extended Langmuir (*dashed line*) and MREL combinated with Dualsite Langmuir model (*solid line*) are also plotted

Table 2 Parameters of CO_2 obtained by fit to dualsite Langmuir model

	Dualsite Langmuir model				
	q_{m1}	b_1	q_{m2}	b_2	%D
S15	0.011	0.161	0.089	3.164	12.66
STMB	0.010	0.184	0.091	4.756	7.17
SHEPF	0.007	0.161	0.115	15.54	4.49
STMBF	0.006	0.165	0.109	3.839	3.94

Deviations between fitted data and experimental data is also shown

q_m: maximum adsorption capacity, q_m in g/g and b in bar^{-1}

CO_2/mol CH_4 until 25 and 28 respectively. A higher concentration of amine groups on the silica surface significantly improve the selectivity towards CO_2 adsorption. Although amino functionalized mesoporous silicas show values for CO_2 adsorption relatively lower than other adsorbents such as carbons, the superior CO_2/CH_4 selectivity and the high adsorption capacity at higher temperatures justify efforts on its study (Fig. 6).

Kinetic measurements for CO_2 adsorption were carried out for the four grafted silicas under study. By fixing CO_2 pressure (0.2 bar) and temperature (25 °C), the sample mass gain was registered as a function of time until equilibrium mass was reached at this pressure. The kinetic curves in Fig. 7 clearly show that more ordered materials reach adsorption equilibrium faster (90 % of equilibrium adsorbed concentration is reached in 22, 15, 94 and 92 min for SBA, STMB, SHEPF and STMBF, respectively). It is generally accepted that CO_2 adsorption on amino silicas is limited by (a) a hampered diffusion through the amino layer of the adsorbent (Bollini et al. 2012), (b) a slower reaction of CO_2 with secondary amino groups as compared to primary amino groups (Harlick and Sayari 2006) and

Table 3 Parameters of CO_2 and CH_4 obtained by fit to Langmuir model

	Langmuir model						
	CO_2		CH_4		EL	MREL	MREL DL
	q_m	b	q_m	b	%D	%D	%D
S15	0.101	1.871	0.011	0.292	7.12	12.44	7.10
STMB	0.099	2.943	0.010	0.281	9.76	8.91	7.62
SHEPF	0.118	5.214	0.007	0.212	5.27	4.81	4.92
STMBFF	0.105	3.014	0.006	0.185	12.21	9.19	3.39

Deviations between EL, MRLE and MRLE combined with DsL data and mixture experimental data is also shown

q_m: maximum adsorption capacity, q_m in g/g and b in bar^{-1}

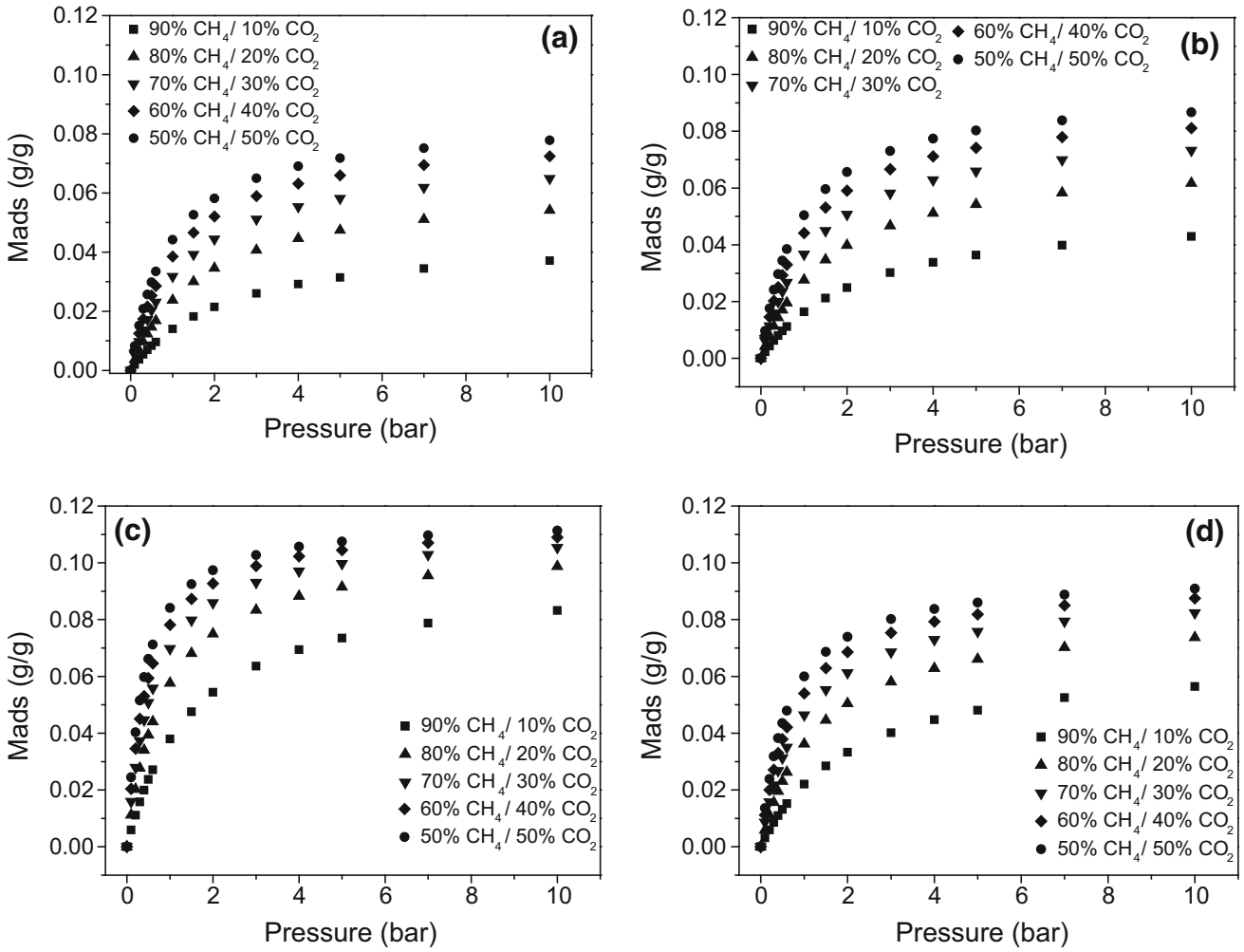

Fig. 5 Simulated isotherms at 25 °C from Multiregion extended Langmuir combined with Dualsite Langmuir model for several CO_2/CH_4 mixtures **a** SBA15, **b** STMB, **c** SHEPF and **d** STMBF

(c) the chemical rearrangement from carbamate to carbonate species in the presence of water (although this only applies when moisture is present) (Serna-Guerrero et al. 2008). In this case, amino functionalization was carried out with APTES, which supplied only primary amines to the surface and CO_2 uptake was carried out at anhydrous conditions. Therefore, the only consideration left to explain the different kinetic behavior in samples is the hindered diffusion caused by a higher density of grafted APTES molecules. The higher grafting yield of less ordered

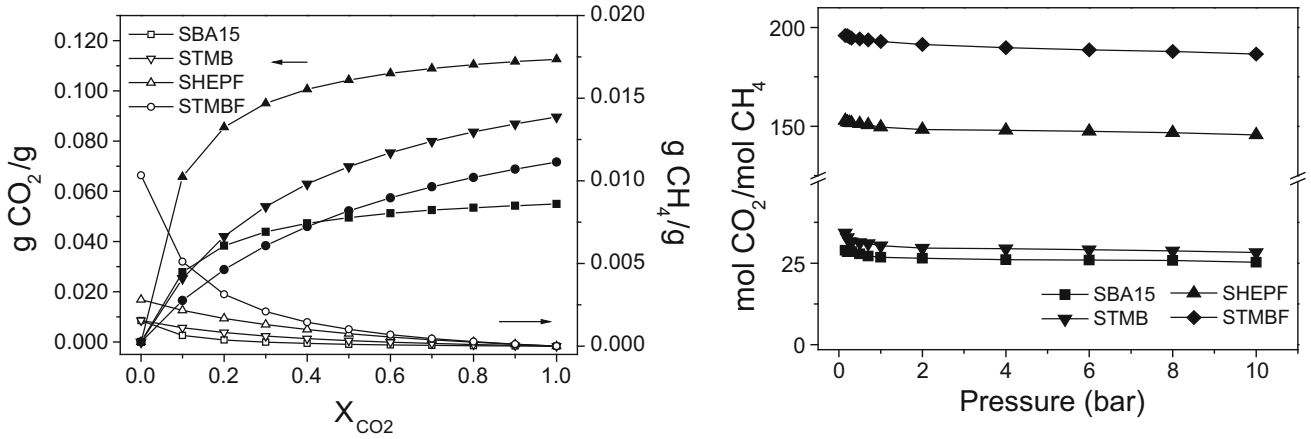

Fig. 6 Quantity of adsorbed CO_2 and CH_4 as a function of CO_2 molar ratio at 1 bar (obtained from Langmuir extended model) (*left*). Molar ratio between adsorbed CO_2 and CH_4 at 25 °C as a function of the pressure

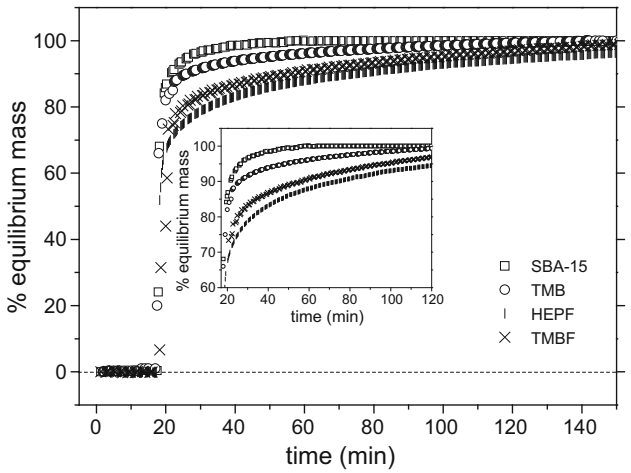

Fig. 7 Time employed to reach the equilibrium mass at 0.2 bar and 25 °C for amino grafted silicas

materials may be explained by the shorter mesochannels, whose growth was limited by the presence of fluoride. This improves the access of APTES molecule to the silanols groups and increases the grafting yield. In addition, other authors (Xing et al. 2012; Bermúdez et al. 2013) have reported that the increase in CO_2 uptake of the N-containing materials could also be related to hydrogen bonding interactions between hydrogen (from C-H and N–H) atoms and CO_2 molecules. This could explain why the q_m values of CO_2 obtained from the DsL model on the high affinity site are lower than the theoretical capacities that would be expected from the %N content from elemental analysis. For example, SBA15 shows a q_m of 0.089 g CO_2/g on site 1, while the adsorbed value should be 0.062 g CO_2/g taking into account the % N content. The difference between these values may be related to the interaction of CO_2 and hydrogen (C–H or/and N–H) atoms from aminopropyl groups, which in turn may lead to slower kinetics. Therefore, kinetic behavior is hindered for a higher density of amino groups and C-H from propyl chains may also increases the necessary time to reach the equilibrium.

5 Conclusions

Mesoporous silicas of SBA-15 type have been synthesized with different pore sizes and mesoscopic arrangement using pore expanders. The use of ammonium fluoride as a solubility enhancer of heptanes resulted in successful expansion of the hydrophobic core of the micelles. To improve the CO_2 affinity of these materials, all of them were functionalized using APTES as amino source. These materials showed high affinity toward CO_2 adsorption at low pressures, and may be regenerated at 120 °C. The incorporation of amine groups led to materials with exceptionally high CO_2/CH_4 selectivity (around 200 mol CO_2/mol CH_4 at 25 °C and 0.2 bar). Multi Region Extended Langmuir model applied along with Dual site Langmuir model was successfully used to predict the mixture behavior of these samples, showing a greater accuracy for all samples as compared to Extended Langmuir and simple Dual Site Langmuir. Due to a higher grafting yield, large pore and less ordered materials showed not only a higher CO_2 uptake, but also higher CO_2/CH_4 selectivity. On the other hand, adsorption kinetics was slower in such materials due to hindered diffusion caused by a high density of grafted moieties.

Acknowledgments We thank project CTQ2012-37925-C03-03 (Ministerio de Economía y Competitividad) and FEDER funds, project RNM 1565 (Excelencia, Junta de Andalucía) and European project 295156 FP7-PEOPLE-2011-IRSES for financial support. E. Vilarrasa-Garcia thanks CAPES/PNPD (Brazilian Ministry of Education) for post-doctoral fellowship.

References

Bai, R., Yang, R.T.: A thermodynamically consistent Langmuir model for mixed gas adsorption. J. Colloid Interf. Sci. **239**, 296–302 (2001)

Barrett, E.P., Joyner, L.G., Halenda, P.P.: The determination of pore volume and area distributions in porous substances. I. Computations from nitrogen isotherms. J. Am. Chem. Soc. **73**, 373–380 (1951)

Beck, J.S., Vartuli, J.C., Roth, W.J., Leonowicz, M.E., Kresge, C.T., Schmitt, K.D., Chu, C.T.W., Olson, D.H., Sheppard, E.W.: A new family of mesoporous molecular sieves prepared with liquid crystal templates. J. Am. Chem. Soc. **114**, 10834–10843 (1992)

Bermúdez, J.M., Dominguez, P.H., Arenillas, A., Cot, J., Weber, J., Luque, R.: CO_2 separation and capture properties of porous carbonaceous materials from leather residues. Materials **6**, 4641–4653 (2013)

Bollini, P., Brunelli, N.A., Didas, S.A., Jones, C.W.: Dynamics of CO_2 adsorption on amine adsorbents. 2. Insights into adsorbent design. Ind. Eng. Chem. Res. **51**, 15153–15162 (2012)

Boissière, C., Larbot, A., Prouzet, E.: Synthesis of mesoporous MSU-X materials using inexpensive silica sources. Chem. Mater. **12**, 1937–1940 (2000a)

Boissière, C., Larbot, A., Van der Lee, A., Kooyman, P.J., Prouzet, E.: A new synthesis of mesoporous MSU-X silica controlled by a two-step pathway. Chem. Mater. **12**, 2902–2913 (2000b)

Brunauer, S., Emmett, P.H., Teller, E.: Adsorption of gases in multimolecular layers. J. Am. Chem. Soc. **60**, 309–319 (1938)

Cao, L., Man, T., Kruk, M.: Synthesis of ultra-large-pore SBA-15 silica with two-dimensional hexagonal structure using triisopropylbenzene as micelle expander. Chem. Mater. **21**(6), 1144–1153 (2009)

Celer, E.B., Jaroniec, M.: Temperature-programmed microwave-assisted synthesis of SBA-15 ordered mesoporous silica. J. Am. Chem. Soc. **128**, 14408–14414 (2006)

Chang, A.C.C., Chuang, S.S.C., Gray, M., Soong, Y.: In-situ infrared study of CO_2 on SBA-15 grafted with γ-(aminopropyl) triethoxysilane. Energy Fuels **17**, 468 (2003)

Dreisbach, F., Staudt, R., Keller, J.U.: High pressure adsorption data of methane, nitrogen, carbon dioxide and their binary and ternary mixtures on activated carbon. Adsorption **5**, 215–227 (1999)

Exxon Mobil: The Outlook of Energy: A View to 2040, 2012. http://corporate.exxonmobil.com/en/energy/energy-outlook

Fornés, V., López, C.H.H., Martínez, A.: Catalytic performance of mesoporous VOx/SBA-15 catalysts for the partial oxidation of methane to formaldehyde. Appl. Catal. A: Gen. **249**, 345–354 (2003)

Fulvio, P.F., Pikus, S., Jaroniec, M.: Short-time synthesis of SBA-15 using various silica sources. J. Colloid Interf. Sci. **287**, 717–720 (2005)

Gunathilake, C., Jaroniec, M.: Mesoporous organosilica with amidoxime groups for CO_2 Sorption. ACS Appl. Mater. Interf. **6**, 13069–13078 (2014)

Harlick, P.J.E., Sayari, A.: Applications of pore-expanded mesoporous silicas. 3. Triamine silane grafting for enhanced CO_2 adsorption. Ind. Eng. Chem. Res. **45**(9), 3248–3255 (2006)

Heydari-Gorji, A., Belmabkhout, Y., Sayari, A.: Degradation of amine-supported CO_2 adsorbents in the presence of oxygen-containing gases. Micropor. Mesopor. Mat. **145**, 146–149 (2011)

Hiyoshi, N., Yogo, K., Yashima, T.: Adsorption of carbon dioxide on modified mesoporous materials in the presence of water vapor. Stud. Surf. Sci. Catal. **154**, 2995–3002 (2004)

Jing, Y., Wei, L., Wang, Y., Yu, Y.: Synthesis, characterization and CO_2 capture of mesoporous SBA-15 adsorbents functionalized with melanine-based and acrylate-based amine dendrimers. Micropor. Mesopor. Mat. **183**, 124–133 (2014)

Kishor, R., Ghoshal, A.K.: APTES grafted ordered mesoporous silica KIT-6 for CO_2 adsorption. Chem. Eng. J. **262**, 882–890 (2015)

Kruk, M., Jaroniec, M., Ko, C.H., Ryoo, R.: Characterization of the Porous Structure of SBA-15. Chem. Mater. **12**, 1961–1968 (2000)

Lackner, K.S., Park, A.H.A., Miller, B.G.: Eliminating CO_2 emissions from coal-fired power plants. In: Sioshansi, F.P. (ed.) Carbon Constrained: Future of Electricity Generation, pp. 127–173. Elsevier, Amsterdam (2009)

Lettow, J.S., Han, Y.J., Schmidt-Winkel, P., Yang, P., Zhao, D., Stucky, G.D., Ying, J.Y.: Hexagonal to mesocellular foam phase transition in polymer-templated mesoporous silicas. Langmuir **16**, 8291–8295 (2000)

McCarty, R.D., Arp, V.D.: A new wide range equation of state for helium. Adv. Cryo. Eng. **35**, 1465–1475 (1990)

Newalkar, B.L., Choudary, N.V., Turaga, U.T.: Potential adsorbent for light hydrocarbon separation: role of SBA-15 framework porosity. Chem. Mater. **15**, 1474–1479 (2003)

Ryoo, R., Ko, C.H., Kruk, M., Antochshuk, V., Jaroniec, M.: Block-copolymer-templated ordered mesoporous silica: array of uniform mesopores or mesopore-micropore network? J. Phys. Chem. B **104**, 11465–11471 (2000)

Sanz-Perez, E.S., Olivares-Marin, M., Arencibia, A., Sanz, R., Calleja, G., Maroto-Valer, M.M.: CO_2 adsorption performance of amino-functionalized SBA-15 under post-combustion conditions. Int. J. Greenhouse Gas Control **17**, 366–375 (2013)

Schmidt-Winkel, P., Lukens Jr, W.W., Yang, P., Margolese, D.I., Lettow, J.S., Ying, J.Y., Stucky, G.D.: Microemulsion templating of siliceous mesostructured cellular foams with well-defined ultralarge mesopores. Chem. Mater. **12**, 686–696 (2000)

Schmidt-Winkel, P., Lukens Jr, W.W., Zhao, D., Yang, P., Chmelka, B.F., Stucky, G.D.: Mesocellular siliceous foams with uniformly sized cells and windows. J. Am. Chem. Soc. **121**, 254–255 (1999)

Serna-Guerrero, R., Da'na, E., Sayari, A.: New insights into the interactions of CO_2 with amine-functionalized sílica. Ind. Eng. Chem. Res. **47**, 9406–9412 (2008)

Setzmann, U., Wagner, W.: A new equation of state and tables of the thermodynamic properties for methane covering the range from the melting line to 625 K at pressures up to 1000 MPa. J. Phys. Chem. Ref. Data **20**, 1061–1155 (1991)

Span, R., Wagner, W.: A new equation of state for carbon dioxide covering dioxide the fluid region from the triple-point temperature to 1100 K at pressures up to 800 MPa. J. Phys. Chem. Ref. Data **25**, 1509–1596 (1996)

Tagliabue, M., Farrusseng, D., Valencia, S., Aguado, S., Ravon, U., Rizzo, C., Corma, A., Mirodatos, C.: Natural gas treating by selective adsorption: material science and chemical engineering interplay. Chem. Eng. J. **155**, 553–566 (2009)

Veawab, A., Aroonwilas, A., Tontiwachwuthikul, P.: CO_2 absorption performance of aqueous alkanolamines in packed columns. Abstr. Pap. Am. Chem. S. **223**, U568–U569 (2002)

Vilarrasa-García, E., Cecilia, J.A., Santos, S.M.L., Cavalcante Jr, C.L., Jiménez-Jiménez, J., Azevedo, D.C.S., Rodríguez-Castellón, E.: CO_2 adsorption on APTES functionalized mesocellular foams obtained from mesoporous silicas. Micropor. Mesopor. Mat. **187**, 125–134 (2014)

Vilarrasa-Garcia, E., Ortigosa-Moya, E.M., Cavalcante Jr, C.L., Jiménez-Jiménez, J., Azevedo, D.C.S., Rodríguez-Castellón, E.: CO_2 adsorption on amine modified mesoporous silicas: effect of the progressive disorder of the honeycomb arrangement. Micropor. Mesopor. Mat. **209**, 172–183 (2015)

Wang, Q., Luo, J., Zhong, Z., Borgna, A.: CO_2 capture by solid adsorbents and their applications: current status and new trends. Energy Environ. Sci. **4**, 42–55 (2011)

Wang, L., Yang, R.T.: Increasing selective CO_2 adsorption on amine-grafted SBA-15 by increasing silanol density. J. Phys. Chem. C **115**, 21264–21272 (2011)

Wolsky, A.M., Daniels, E.J., Jody, B.J.: CO_2 capture from the flue gas of conventional fossil-fuel-fired power plants. Environ. Prog. **13**, 214–219 (1994)

Xing, W., Liu, C., Zhou, Z., Zhang, L., Zhou, J., Zhuo, S., Yan, Z., Gao, H., Wang, G., Qiao, S.Z.: Superior CO_2 uptake of N-doped activated carbon through hydrogen-bonding interaction. Energy Environ. Sci. **5**, 7323–7327 (2012)

Yang, R.T.: Gas Separation by Adsorption Processes. Butterworth, Boston (1987)

Zhang, H., Sung, J., Ma, D., Bao, X., Klein-Hoffmann, A., Weinberg, G., Su, D., Schlogl, R.: Unusual mesoporous SBA-15 with parallel channels running along the short axis. J. Am. Chem. Soc. **126**, 7440–7441 (2004)

Zhao, D., Feng, J., Huo, Q., Melosh, N., Fredrickson, G.H., Chmelka, B.F.: Triblock copolymer syntheses of mesoporous silica with periodic 50 to 300 angstrom pores. Science **279**, 548–552 (1998a)

Zhao, D., Huo, Q., Feng, J., Chmelka, B.F., Stucky, G.D.: Nonionic triblock and star diblock copolymer and oligomeric surfactant syntheses of highly ordered, hydrothermally stable, mesoporous silica structures. J. Am. Chem. Soc. **120**, 6024–6036 (1998b)

Zelenak, V., Halamova, D., Gaberova, L., Bloch, E., Llewellyn, P.: Amine-modified SBA-12 mesoporous silica for carbon dioxide capture: effect amine basicity on sorption properties Micropor. Mesopor. Mat. **116**, 358–364 (2008)